Biosensors and Bioelectronics 219 (2023) 114848

Contents lists available at ScienceDirect

Biosensors and Bioelectronics

journal homepage: www.elsevier.com/locate/bios

Carbon dot based sensing platform for real-time imaging Cu^{2+} distribution in plants and environment

Junjie Lin [a], Xiaoman Huang [a], Erfeng Kou [a], Wenxiao Cai [a], Haoran Zhang [a], Xuejie Zhang [a], Yingliang Liu [a], Wei Li [a,*], Yinjian Zheng [c,**], Bingfu Lei [a,b,***]

[a] Key Laboratory for Biobased Materials and Energy of Ministry of Education, College of Materials and Energy, South China Agricultural University, Guangzhou, 510642, PR China

[b] Maoming Branch, Guangdong Laboratory for Lingnan Modern Agriculture, Guangdong, Maoming, 525100, PR China

[c] Institute of Urban Agriculture, Chinese Academy of Agricultural Science, Chengdu, 610218, PR China

ARTICLE INFO

Keywords:
Biosensor
Cu^{2+} detection
Carbon dots
Plant

ABSTRACT

Divalent copper is a double-edged sword for plants, excess or shortage of copper ions will cause adverse reactions in plants. Currently, Cu^{2+} sensor for plants is still underdeveloped and new technology is urgently required for realizing one-step and real-time detection of Cu^{2+} in plants. Herein, a home-made and low-cost sensing platform is constructed by using carbon dots (CDs) as the optical probe, electronic devices for image acquisition, and a built-in algorithm program for image processing, which allows the dynamic monitoring of Cu^{2+} distribution in different plant species with high spatial and temporal resolution. We found that the detection limit of R-CDs for Cu^{2+} in water sample was 0.375 nM, and 11.7 mg/kg or even less Cu^{2+} in plants can be visually observed and accurately detected by the sensing platform. Moreover, this sensing platform has also been employed for reporting the spatial distribution of Cu^{2+} in the external environment of plants, demonstrating its applicability for monitoring Cu^{2+} both in living plants and the surrounding environment. This study provides a smart sensing platform for precise detection in plant internal and external environments, offering a promising strategy for precision agriculture in real-time and remote-control manners.

1. Introduction

Copper is a necessary trace element for the growth of plants, which also serves as an important component of various proteins and enzymes, combining with enzymes to perform many nutritional functions. When crops are deficient in copper, photosynthetic activity will be inhibited and protein synthesis will be affected, resulting in dwarfing, sterility, and yield reduction (Dubey et al., 2018; Hossain et al., 2012). On the other hand, the damage of excessive copper on plants is mainly manifested in reducing the membrane integrity and enzyme activity of photosystem II (PS II), affecting the chlorophyll synthesis and the efficiency of main photochemical reactions (Jin et al., 2021). Copper mostly exists as Cu^{2+} in an aqueous environment, and Cu^{2+} is the main chemical form of copper that is adsorbed by plants (Lu et al., 2017a,b; Ouzounidou, 1994). Currently, precision agriculture is an important strategy to reduce the toxic stress of heavy metals in crops, which is of great significance for plant growth (Kupper and Andresen, 2016). Precision agriculture aims to use sensing technology to detect chemical signals that may cause crop stress in the early stage, and solve the problem of annual reduction of arable land by optimizing the production mode and crop yield (Fichman et al., 2019; Zarco-Tejada et al., 2018). For maintaining plant homeostasis, it is necessary to design a sensitive, rapid, and real-time biosensor to dynamically detect the absorption of Cu^{2+} and its spatial distribution in plants.

Previously reported Cu^{2+} sensing methods in plants are not user-friendly. The traditional method for copper detection is based on inductively coupled plasma (Bersier et al., 1994; Kin et al., 2016). Although this method has high accuracy, it causes damage to plants, requires a large number of samples, and suffers from cumbersome testing procedures. Commonly, the methods for the determination of

* Corresponding author.
** Corresponding author.
*** Corresponding author. Key Laboratory for Biobased Materials and Energy of Ministry of Education, College of Materials and Energy, South China Agricultural University, Guangzhou, 510642, PR China.
E-mail addresses: liwei@scau.edu.cn (W. Li), zhengyinjian@caas.cn (Y. Zheng), tleibf@scau.edu.cn (B. Lei).

https://doi.org/10.1016/j.bios.2022.114848
Received 10 August 2022; Received in revised form 21 September 2022; Accepted 20 October 2022
Available online 23 October 2022

Cu^{2+} in plants involve conventional field sampling, plant sample digestion, and atomic absorption spectrophotometry analysis. These methods require expensive instruments, professional operators, and complex pretreatments, and are not conducive to monitoring copper absorption in real-time. Although nanomaterial-based probes for Cu^{2+} detection have been developed, such as carbon dots (Chen et al., 2016; Ge et al., 2021; Gedda et al., 2016), rhodamine (Rasheed et al., 2019; Zhang et al., 2007), polydopamine based nanoparticle (Su et al., 2016), chrysosplenol-D (Saleh et al., 2020), these studies were only carried out in the solutions or mammal cells (Gedda et al., 2016), rather than spatially locating Cu^{2+} in entire plants and their culture environments. In recent reports, nanomaterials have been used to detect glucose (Li et al., 2018a,b), nitroaromatics (Wong et al., 2017), and H_2O_2 (Lew et al., 2020) in plants by foliar infiltration. However, *in vivo* and *in vitro* detection that collaborative the imaging of the ion absorption between plants system and their growing environment is scarcely reported. At present, no technique can sensitively and visually realize Cu^{2+} mapping in plant systems and monitor Cu^{2+} concentration statistically through simple devices in case plant lesions occur. Therefore, it is promising to develop a smart sensing platform to dynamically monitor Cu^{2+} in plants and the surrounding environment.

Fluorescent carbon dots (CDs) have attracted much attention because of their fascinating photoluminescence and stable physiochemical properties (Li et al., 2018a,b), which show great potential as optical nanosensors in biosystems (Lu et al., 2017a,b; Nissler et al., 2022). Compared with other nanoprobes, CDs are superior to semiconductor quantum dots (QDs), organic dyes, metal-doped nanoparticles, and carbon nanotubes in terms of their good biocompatibility, excellent water solubility, and small size. Despite CDs having been intensively studied in mammalian systems (Liu et al., 2021), CD-based nanosensor has not been reported in living plants. In this work, a home-made Cu^{2+} sensing platform for plant systems was constructed with bright red fluorescent carbon dots (R-CDs) as the nanosensor and electronic devices as the signal readout tool (Fig. 1). The R-CDs taken up by the roots and transported along the plant vasculature are sensitive to Cu^{2+}, from which the fluorescence quenching can be dynamically imaged by electronic devices and processed by a built-in algorithm program, realizing the real-time visualization of Cu^{2+} distribution inside plants and recording related intensity. Besides, this sensing platform is also applicable for sensing Cu^{2+} in the surrounding environment to determine the heavy metal contamination around the plants. This study provides a highly effective sensing platform for non-destructive detection of Cu^{2+} in plants and the environment with high spatial and temporal resolution, presenting a promising strategy for synergetic monitoring of plant health and environmental contamination.

2. Results and discussion

2.1. High sensitivity and selectivity of R-CDs toward Cu^{2+}

R-CDs were synthesized from formamide and glutathione based on a modified method (Pan et al., 2016), which are quasi-spherical and well dispersed with an average size of ~2.91 nm (Fig. S1). The lattice spacing of 0.21 nm (inset of Fig. S1A) is in accordance with the (100) facet of graphite and reveals the graphite-like structure in R-CDs (Pan et al., 2016). The particle size (hydrodynamic diameter) of the R-CDs solution was 344.33 ± 50.54 nm and the zeta potential was −16.1 mV (Fig. S2), indicating that R-CDs had good water solubility (Ahmed et al., 2021; Moradi et al., 2018; Pan et al., 2020). The small particle size and good water solubility of R-CDs make them possible to translocate within the plant system. Then, optical properties of R-CDs were further investigated. R-CDs have bright red emission peaked at 680 nm under the optimal excitation of 420 nm (Fig. 2A), which also features an excitation-independent emission behavior (Fig. 2B) (Nie et al., 2014). Upon the addition of Cu^{2+} with concentrations from 1 to 20 nM, the bright red fluorescence of R-CDs gradually quenched (Fig. 2C), which can be clearly observed by the naked eyes under the UV lamp ($\lambda_{ex} = 365$ nm) as shown in Fig. 2D. Accordingly, in Fig. 2E, the fluorescence quenching plots were linearly fitted with the equation: $y = 0.04\,x + 1$ (x: c_{Cu}^{2+}: nM, $R^2 = 0.999$). The limit of detection (LOD) for Cu^{2+} was calculated by the equation of LOD = 3σ/s, where σ is the standard deviation of blank groups (n = 9) and s is the slope of the curve (Dong

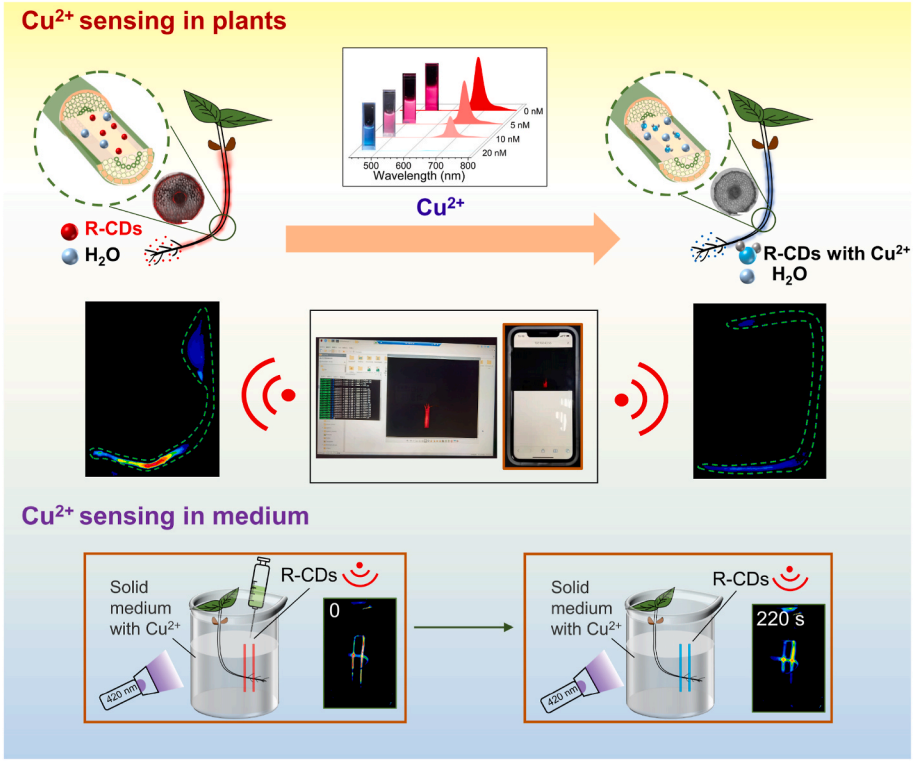

Fig. 1. Schematic diagram of R-CDs based sensing platform for detecting Cu^{2+} in plants and the external environment. The as-prepared R-CDs exhibit fluorescence quenching behavior upon interaction with Cu^{2+}. For sensing Cu^{2+} in plants, R-CDs were absorbed by plant roots and then translocated into the stem to sense inner Cu^{2+}. For sensing Cu^{2+} in the medium, R-CDs were injected into the medium to detect Cu^{2+} around the root. The Cu^{2+} distribution inside the plant as well as the outer medium was imaged by the sensing platform and a camera or mobile phone was connected for real-time monitoring.

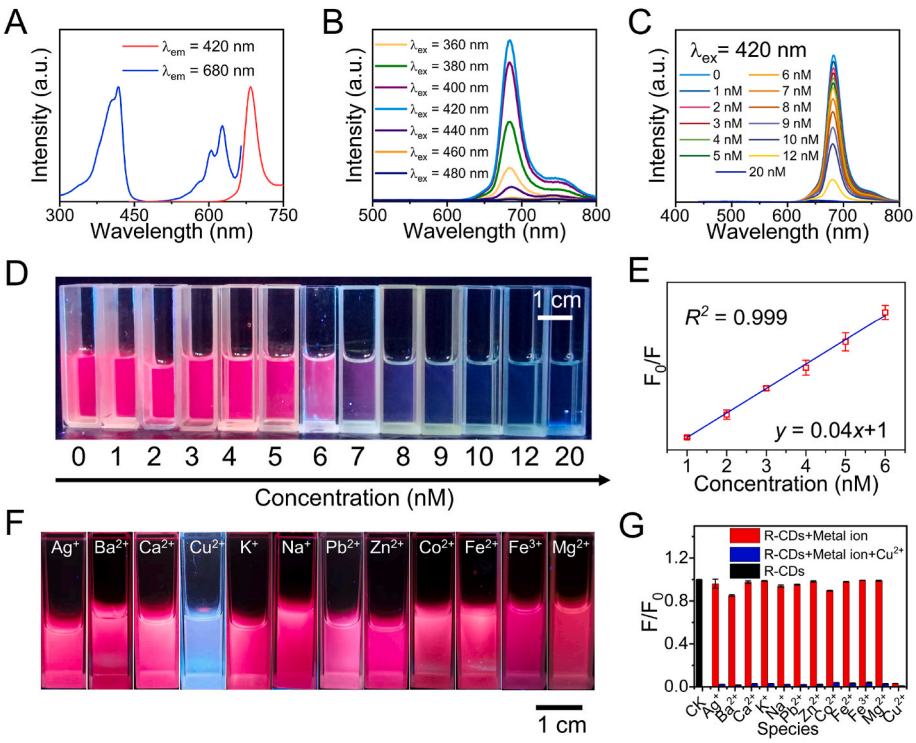

Fig. 2. (A) Excitation and emission spectra of R-CDs; (B) Emission spectra of R-CDs under different excitation wavelengths; (C) Fluorescence spectra of R-CDs at different Cu^{2+} concentrations; (D) Photographs of R-CDs solution with different concentrations of Cu^{2+} under a 365 nm UV lamp. The concentrations are 0, 1, 2, 3, 4, 5, 6, 7, 8, 9, 10, 12, and 20 nM from left to right; (E) The calibration curves of fluorescence quenching effects of R-CDs by different concentrations of Cu^{2+}, F_0 and F are the maximum fluorescence intensity of R-CDs without and with Cu^{2+}, respectively; (F) Photographs of R-CDs solution with various metal ions respectively under the excitation of a 420 nm lamp. Images are processed by 645 nm filtering. [R-CDs] = 10 mg/L, [Cu^{2+}] = 20 nM, [metal ions] = 20 nM; (G) Fluorescence response of R-CDs toward Cu^{2+} and various metal ions, λ_{ex} = 420 nm, [R-CDs] = 10 mg/L, [Cu^{2+}] = 20 nM, [metal ions] = 20 nM.

et al., 2020; Du et al., 2021; Liu et al., 2021; Yan et al., 2018). The LOD for Cu^{2+} reaches 0.375 nM in the range of 1–6 nM. We made a comparison of LOD of the previously reported methods (Table S1) and it clearly demonstrated the ultra-sensitive detection of Cu^{2+} by R-CDs. In order to explore their capability of acting as an optical sensor for metal ion detection, the fluorescence response of R-CDs towards various metal ions such as Ag^{+}, Ba^{2+}, Ca^{2+}, K^{+}, Na^{+}, Pb^{2+}, Zn^{2+}, Co^{2+}, Fe^{2+}, Fe^{3+}, and Mg^{2+} was investigated. As shown in Fig. 2F–G, among various metal ions respectively, only Cu^{2+} caused a significant fluorescence quenching implying that the R-CDs could be employed as a turn-off chemo-sensor for the selective detection of Cu^{2+}. Anti-interference ability is an important evaluation for practical applications of sensing probe (Xu et al., 2015). Anti-interference ability was studied by recording the emission spectra in the co-presence of Cu^{2+} and other metal ions. As shown in Fig. 2G, the presence of other metal ions will not affect the detection of Cu^{2+} by R-CDs, which proves that R-CDs have excellent anti-interference ability. Considering the high content of some elements in plant internal environment, we explored the effect of common elements on R-CDs fluorescence at 10 times concentration (200 nM). The results were consistent with the above conclusions. The spectrogram shows that only Cu^{2+} causes a large degree of fluorescence quenching, and the other ions have less than 10% effect on fluorescence (Fig. S3). At the same time, the response of R-CDs to Cu^{2+} was not affected by the high concentration of interfering ions. In addition, in the presence of amino acids and glucose, R-CDs also showed excellent selectivity in detecting Cu^{2+} (Fig. S4). In general, R-CDs are a fluorescent sensor with high anti-interference ability and specific and sensitive response to Cu^{2+} (Wang et al., 2017).

Liang et al., (2021) demonstrated that the dehydration reaction of unsubstituted amide bond and carboxyl group is the key to the formation of red fluorescent carbon dots. Glutathione has carboxyl groups at both ends similar to citric acid, which can dehydrate with the amino group of formamide, and further polymerize and carbonize at high temperature to form R-CDs (Chen et al., 2020; Wei et al., 2020). Nitrogen doping makes the fluorescence gradually red-shifted by introducing a lower energy level (Holá et al., 2017; Nie et al., 2014). While the addition of Cu^{2+} will cause the obvious quenching of red fluorescence. Furthermore, the relationship between the amount of nitrogen doping and the detection effect of Cu^{2+} was investigated. The amount of nitrogen doped was regulated by controlling the amount of formamide (glutathione: formamide = 1:1, 1:2, 1:3). XPS results showed that the nitrogen content of R-CDs increased gradually with the increase of formamide (Fig. S5). As shown in Fig. S6, the fluorescence intensities decreased at different rates with the increase of Cu^{2+} concentration and were finally completely quenched. The decline rate of fluorescence intensities displays signs related to the amount of doped nitrogen. The group at the ratio of 1:1 shows a rapid decrease in fluorescence intensity in 1–4 nM Cu^{2+} solution, while the group at the ratio of 1:3 shows a rapid quenching phenomenon in 3–6 nM Cu^{2+} solution. The results demonstrate that low doping amounts are easily quenched by Cu^{2+}, while high doping amounts have a higher tolerance to Cu^{2+}. In the group at the ratio of 1:2, fluorescence quenching showed a good linear relationship with the concentration of Cu^{2+}. Therefore, R-CDs used below were synthesized at a ratio of 1:2. The results prove that the quenching effect of R-CDs on Cu^{2+} is related to nitrogen.

To gain insight into the quenching mechanism, the fluorescence response of R-CDs toward Cu^{2+} was further investigated. Fluorescence quenching is generally considered to be caused by fluorescence resonance energy transfer (FRET), inner filter effect (IFE), dynamic quenching (DQE) and static quenching (SQE) (Bozkurt et al., 2013; Li et al., 2014). Since negligible overlap between the absorption band of Cu^{2+} and the fluorescence spectrum of R-CDs (Fig. S7), the effect of IFE or FRET could be ruled out (Zhai et al., 2014). Then, the fluorescence quenching behavior was described by the Stern-Volmer equation.

$$F_0/F = 1+K_{SV}[Cu^{2+}] \quad (1)$$

where, [Cu^{2+}] is the concentration of the quenching agent in the system, F and F_0 represent the fluorescence intensities of R-CDs in the presence and absence of Cu^{2+}, respectively.

As revealed in Fig. S8, the Stern-Volmer plot followed a good linear trend with Cu^{2+} concentration and the Stern-Volmer quenching constant (K_{sv}) was found to be 4.37×10^{7} mol^{-1} L. Dynamic or static quenching can be discriminated by studying the relationship between quenching constant and temperature. When the temperature of the system rose

from 25 to 50 °C, the quenching constant of the reaction increased from 4.37×10^7 to 14.26×10^7 mol^{-1} L (Fig. S8). As we all know, with the increase of temperature, the Brownian motion of molecules becomes more intense, and the number of collisions between Cu^{2+} and R-CDs in the system increases. Hence, the phenomenon that the quenching constant is proportional to temperature can be attributed to its dynamic properties (Lu et al., 2018). To further study the quenching mechanism, time resolved fluorescence decay analysis was performed on R-CDs. As shown in Fig. S9, the average lifetimes of R-CDs are reduced by 20% (from 4.455 ns to 3.543 ns), which confirms that the dynamic quenching plays a major role in such a quenching process (Li et al. 2020a,b, 2021). From the above results, we proposed a feasible quenching mechanism. First, the surface functional groups of R-CDs form molecular contact with Cu^{2+} through electrostatic adsorption. Then, during violent molecular collisions, nonradiative electron transfer from the excited state of R-CDs to the vacant d orbitals of Cu^{2+}, resulting in the quenching of fluorescence (Bandi et al., 2018; Liu et al., 2018).

2.2. Applicability of R-CDs sensing Cu^{2+} within plants

The highly sensitive and selective sensing abilities toward Cu^{2+} render R-CDs with great potential as a plant sensor. For plant system, conduction is an important mode of nutrient substance transport in plants, which is conjointly accomplished by the main parts of roots, stems, and leaves. Plants first absorb water containing dissolved minerals and inorganic salts through the cells of the root hair. The presence of the Casparian strip in the endodermis makes it necessary for water and solutes to pass through the selective permeable plasma membrane of the endodermis cells into the protoplasm, and then into the vascular bundles. Similarly, R-CDs dissolved in deionized water can be absorbed by plants as organic matter through roots and then translocated upward through the vascular systems because of their small size and good water-solubility. After the co-culturing of 3-day-old bean sprouts with R-CDs solution (20 mg/L) for 2 h, obvious red fluorescence in the xylem of vascular bundle was revealed by confocal images (Figs. S10A and S11A), while no fluorescence can be observed in the control group (Figs. S10B and S11B), which demonstrates that R-CDs can be successfully embedded in plants, offering the possibility for R-CDs to interact with Cu^{2+} within plants. Meanwhile, the route of R-CDs entering plants and the location of aggregation were analyzed by confocal laser images. We found that the red fluorescence signal mainly came from the epidermis and endodermis, and a little from the xylem of vascular tissue. The results show that R-CDs contacted the epidermis, were absorbed by root hair, and then entered into plant cells through osmotic pressure, transported by vascular tissue, and accumulated in the endodermis. In nature, Cu^{2+} mainly exists in soil in the form of hydrate, likewise, it is absorbed by plant roots with water and transported to various organs of the plant through vascular bundles. It is noteworthy that plants have a self-protection mechanism to cope with excess Cu^{2+}, that is, by accumulating Cu^{2+} in the roots and preventing their translocation to the shoots (Thounaojam et al., 2012). Hence, root is the main site where Cu^{2+} enter the plant and accumulate, and the content of Cu^{2+} in the whole plant can be learned by detecting the root. Herein, Cu^{2+} absorbed by roots can interact with R-CDs embedded in Casparian strip to quench the red fluorescence and achieve visual detection of Cu^{2+} in plants. In addition, the toxicity of R-CDs in plants was detected by fluorescein diacetate (FDA) staining. Confocal images show that most cells can be stained, which proves the good viability of bean sprouts incubated with R-CDs (20 mg/L) after 3 h (Fig. S12). The low toxicity of R-CDs has also been reported in our previous report, with a 92% survival rate in Hela cells treated with R-CDs tested with Cell Counting Kit-8 (CCK-8) (Li et al., 2020a,b). Besides, Li et al. also reported that R-CDs can increase the yield of lettuce through light conversion (Li et al., 2020a,b). The above results demonstrate that R-CDs can act as a biocompatible nanosensor within plants.

To demonstrate the applicability of R-CDs nanosensor *in vivo* in plants, the experiments were carried out by culturing 3-day-old bean sprouts in R-CDs solution for 2 h and then transferred into Cu^{2+} solution (50 nM) for 30 min followed by three times wash using deionized water. Confocal images show no obvious red fluorescence, indicating that Cu^{2+} in the plant could quench the red emission of R-CDs (Figs. S10C and S11C). The above results manifest that R-CDs could enter the plant through roots. The other substances within plant, such as amino acids, vitamins, and monosaccharides, would not affect the fluorescence of R-CDs. The successful detection of Cu^{2+} was realized on the microscopic scale.

To realize real-time sensing for Cu^{2+} in living plants or tissues, we used a smart phone with 50-million pixels and a 645 nm filter to collect the fluorescence signal of R-CDs in plants. This simple detection system can be practically applied for tracing Cu^{2+} from root absorption and further infiltration in plant tissues. We chose bean sprouts and spinach as model plants because of their fast growth rate. Onion was selected for plant tissue model because its cells are obvious, which is conducive for observation. By using the setup, plants without R-CDs treatment exhibited negligible background signals after applying Cu^{2+} (Fig. S13). After the treatment of R-CDs and Cu^{2+}, as shown in Fig. 3A–C, the fluorescence intensity in R-CDs treated bean sprouts decreased over time as Cu^{2+} (50 nM) was gradually absorbed and transported into vascular bundle through roots from the solution, similar sensing performance can also be observed in different plant species like the white onion tissue (Fig. 3D–F) as well as spinach (Fig. 3G–I). Statistically, in Fig. 3C and I, the fluorescence intensities recorded from bean sprouts and onion tissue show that the fluorescence intensities dropped significantly after being cultured in Cu^{2+} solution for about 10 min, which were about 50% lower than the original value. While the quenching rate of R-CDs in spinach is slightly slower than other groups (Fig. 3F). The difference is caused by the different affinity of different plant species and tissues for Cu^{2+}, which can be related to the difference in absorption capacity caused by the strength of transpiration (Adamchuk et al., 2004; Salah and Barrington, 2006). Nevertheless, the fluorescence intensities of all plant samples show a consistent downward trend over time, suggesting that R-CDs are still sensitive enough to detect and trace Cu^{2+} inside their biosystems. The results demonstrate that the detection of Cu^{2+} in plants can be visualized by camera and ImageJ image processing software, demonstrating the different absorption rates of Cu^{2+} in different species. Furthermore, the Cu^{2+} content levels and fluctuations in plants were investigated. To begin, the Cu^{2+} contents of spinach roots treated with deionized water, 25 nM, and 50 nM Cu^{2+} solutions for 30 min were determined using inductively coupled plasma spectroscopy (ICP). Meanwhile, the fluorescence changes of R-CDs treated spinach roots were recorded in the corresponding solution for 30 min. Compared with the results in Table S2 and Fig. S14, with the increase of Cu^{2+} culture concentration, the accumulation of Cu^{2+} in spinach roots showed a significant increase from 3.1 mg/kg to 11.7 mg/kg and 18.0 mg/kg, respectively. Accordingly, through the analysis of the images (Fig. S14C, F and I), the change of fluorescence intensity also showed a consistent trend, and the quenching rate of fluorescence intensity increased from ~9% to ~25% and ~60%, respectively. R-CDs are herein demonstrated to be able to detect Cu^{2+} inside plants when plants absorb 25 nM of Cu^{2+} from the surrounding environment. These results prove that low Cu^{2+} levels and fluctuations in plants caused by ambient concentrations can be sensitively detected by R-CDs.

2.3. Construction of sensing platform for real-time monitoring Cu^{2+} in vivo

Like in the previous reports (Lew et al., 2020; Li et al., 2018a,b; Wang et al., 2020; Wu et al., 2020), in order to present the fluorescent change more intuitively, the fluorescence image usually undergoes post-image processing to produce the final false-color image. This complex post-processing conflicts with the requirements of timely and fast monitoring of the analyte. Therefore, we constructed a user-friendly

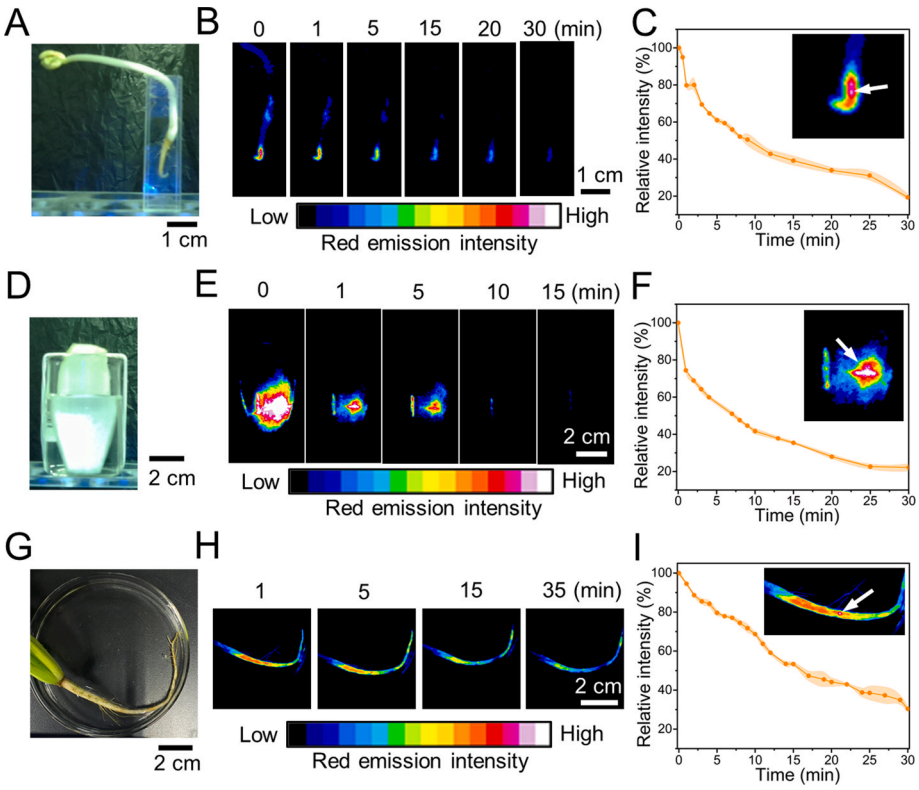

Fig. 3. R-CDs detect Cu^{2+} in living plants or tissues. Images of R-CDs treated bean sprouts (A), white onion tissue (D) and spinach (G) under white light. False color images of absorbed Cu^{2+} detected by R-CDs in bean sprouts (B), white onion tissue (E) and spinach (H) under 420 nm excitation over time. Time profiles of fluorescence intensities of R-CDs in bean sprouts (C), white onion tissue (F) and spinach (I) over time. The white arrows in the inset indicate the measurement points for fluorescence intensities collecting. The shaded regions in (C), (F) and (I) represent the standard deviation from three times sampling.

sensing platform by installing the imaging algorithm program into the camera to directly obtain the false-color image without any further post-processing. In addition, the fluorescence intensity of region of interest could be given, rendering the sensing platform with high accuracy. Herein, this easy-to-use and low-cost sensing platform is assembled by embedding R-CDs as the optical sensor, high-definition camera or mobile phone as the image acquisition tool and the built-in algorithm program as the processing tool, for realizing the dynamic monitoring of Cu^{2+} distribution and relative intensity readout in one step (Fig. 4), the designed operation interface can easily monitor and image the red fluorescence of R-CDs with RGB color value, achieving remote and long-term monitoring of analyte *in vivo* and *in vitro* (Fig. S15). At the same time, the smart phone device can control the functions of the sensing platform and monitor the red fluorescent image through the network connection. Compared with the reported work, this sensing platform is free from manual processing of images, improves the speed of data output and truly realizes the real-time monitoring of analytes.

This sensing platform highlights the timely and rapid response to the analyte reflected by the change of fluorescence signal. Taking living spinach and white onion tissue as examples, during the observation period of 30 min, the fluorescence signals of R-CDs were significantly weakened when R-CDs pretreated spinach (Fig. 5A) and white onion tissue (Fig. 5B) that cultured in Cu^{2+} solution, respectively. In the control group, the fluorescence of R-CDs remained stable when R-CDs pretreated samples that without Cu^{2+} treatment under the same conditions (Fig. 5B and S16). In order to study the autofluorescence effect, spinach without R-CDs treatment was observed under the identical conditions, which showed negligible fluorescence that would not

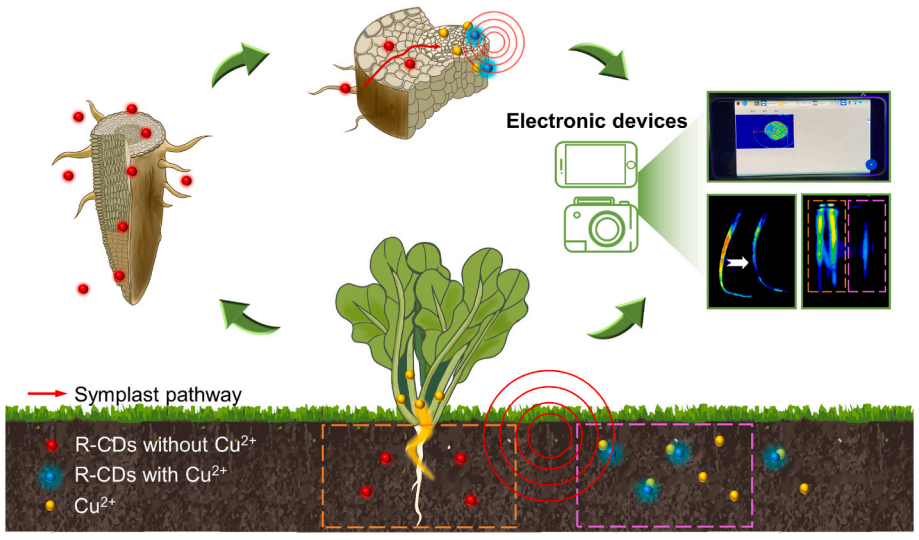

Fig. 4. Schematic diagram of the sensing platform for detecting Cu^{2+} within plants and environment. R-CDs and Cu^{2+} can be translocated into the plant systems via symplast pathway, which induces fluorescence quenching of R-CDs upon interaction. The residual Cu^{2+} in the environment can also be detected by R-CDs. The home-made camera setup directly monitors the changes of the fluorescence signal, processes the image through the built-in algorithm, and finally outputs the results through the external display screen or the connected smart phone, realizing the remote and rapid monitoring of the analyte.

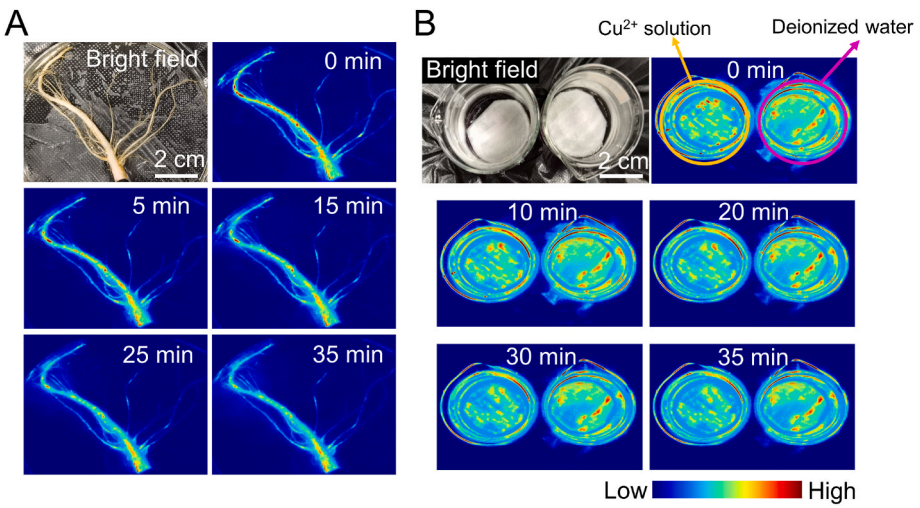

Fig. 5. Real-time detections of Cu^{2+} in plant samples by the sensing platform. (A) Images of R-CDs pretreated spinach that immersed in Cu^{2+} solution (50 nM) over time under white light and 420 nm excitation. (B) Images of R-CDs pretreated white onion tissue that immersed in Cu^{2+} solution (50 nM) (left) and deionized water (right) over time under white light and 420 nm excitation, respectively.

interfere with R-CDs fluorescence (Fig. S17). The above results prove that the home-made sensing platform can successfully record fluorescence signal and output the high-contrast false-color image.

2.4. Monitoring of Cu^{2+} in surrounding environment

Besides monitoring plant inner environment, it is necessary to detect the external growth environment for the sake of plants and even human health. In recent years, soilless cultivation technology has provided an important solution in solving the shortage of cultivated land and increasing crop yields (Ahn et al., 2021; Steffen et al., 2015). As a new culture substrate for soilless culture, hydrogel has been widely studied for its culture effects equal to or even better than soil (Neethu et al., 2018; Ragaveena et al., 2021; Tang et al., 2014). We selected solid medium to simulate the hydrogel environment for plants growth, because solid medium can provide a solid growth environment similar to hydrogel. The detection of Cu^{2+} in the culture environment is conducive to a deeper understanding of plant growth, and provides a significant ion monitoring platform for soilless culture and precision agriculture. First, we tested the detection performance of R-CDs in the solid medium without plants. Specifically, we prepared an AGAR medium with Cu^{2+} concentration of 30 nM and then used a medical needle to inject R-CDs into the medium at the regions of interest. Under the 365 nm UV irradiation, the red fluorescence quenching phenomenon was observed over time (Fig. S18A), indicating that R-CDs fluorescence can be quenched by Cu^{2+} in the environment. Reversely, R-CDs (10 mg/L) were first embedded into the medium, the entire medium showed uniformly red fluorescence under the UV lamp (Fig. S18B), and then Cu^{2+} solution (30 nM) was injected into the medium at certain sites, which appeared as dark dots. These results prove that R-CDs are capable of site-specific detection of Cu^{2+} in the solid environment.

The detection ability of R-CDs in solid media can be further applied to monitor Cu^{2+} uptake by plants from surrounding environment. In the growing process, plants absorb nutrients from the environment through the roots. When plant roots absorb Cu^{2+} from the environment, the residual Cu^{2+} near the root would be less than that of the far root. When R-CDs were injected, the quenching rate of R-CDs would be different due to the different concentration of Cu^{2+} in these two parts. By recording the fluorescence intensities of R-CDs, we can observe the specific location of Cu^{2+} uptake around the roots statistically. Herein, we investigated the concentration changes of Cu^{2+} in the medium after 12-h absorption by plants. As shown in Fig. S19, 4-day-old bean sprouts cultured in deionized water were transplanted into solid AGAR medium containing 30 nM Cu^{2+} for fixation. The as-prepared medium theoretically had uniform Cu^{2+} distribution. After 12-h culture, in order to detect the Cu^{2+} distribution in the medium, R-CDs were injected into the parts of medium near and far from bean sprouts in the same plate, respectively. After 60 s, the red fluorescence around bean sprouts was much stronger than that on the other side far from bean sprouts, indicating the difference in Cu^{2+} concentrations caused by plant absorption. Actually, during the 12-h cultivation, the roots of bean sprouts would absorb water and nutrients, including Cu^{2+} from the medium, thereby reducing external Cu^{2+} concentration around them and causing less fluorescence quenching of R-CDs. These results prove that R-CDs can be used as an optical sensor to preliminarily monitor Cu^{2+} absorption by plants from the surrounding environment.

To demonstrate the applicability of the sensing platform, monitoring and imaging Cu^{2+} uptake at the regions of interest around roots were dynamically imaged and statistically recorded. As shown in Fig. 6, the 3-day-old bean sprout was implanted into solid medium containing Cu^{2+} for 12-h culturing. Then, two 2.5 cm liquid columns of R-CDs were injected into the site close to the root of bean sprout by a medical needle (Fig. 6A–B), and the fluorescence changes were imaged and recorded by the sensing platform with smart phone. It is obvious that the fluorescence intensity in the site far from root decreased significantly due to the unabsorbed Cu^{2+}, while the fluorescence intensity of the near root remained at a high level because of the lower Cu^{2+}(Fig. 6D). In order to make a clear comparison, red fluorescence intensities at the red (near root) and white circles (far from root) were recorded over time (Fig. 6C). After 220 s, the fluorescence intensity in the near-root site remained 70% of the original, while it decreased to 20% in the far-root site. The result shows that the concentration of Cu^{2+} gradually decreased when getting closer to the root along the Z-axis, realizing site-specific Cu^{2+} monitoring around roots. Then, the detection effect in X-axis direction was evaluated. Similarly, as revealed in Fig. 6E–H, fluorescence quenching degree of R-CDs in the site that far from root was as about twice as that of the near root at 170 s, again demonstrating that R-CDs are able to detect the analyte remained in the environment. Experiments *in vitro* monitor the environment after plants absorb Cu^{2+}, while experiments *in vivo* monitor the absorption of Cu^{2+} in plants. The above two experiments realize the collaborative monitoring of Cu^{2+} uptake by plants and improve the accuracy of monitoring. This sensing platform provides great promise for determining environmental contamination and monitoring synergetic plant health spatially and temporally.

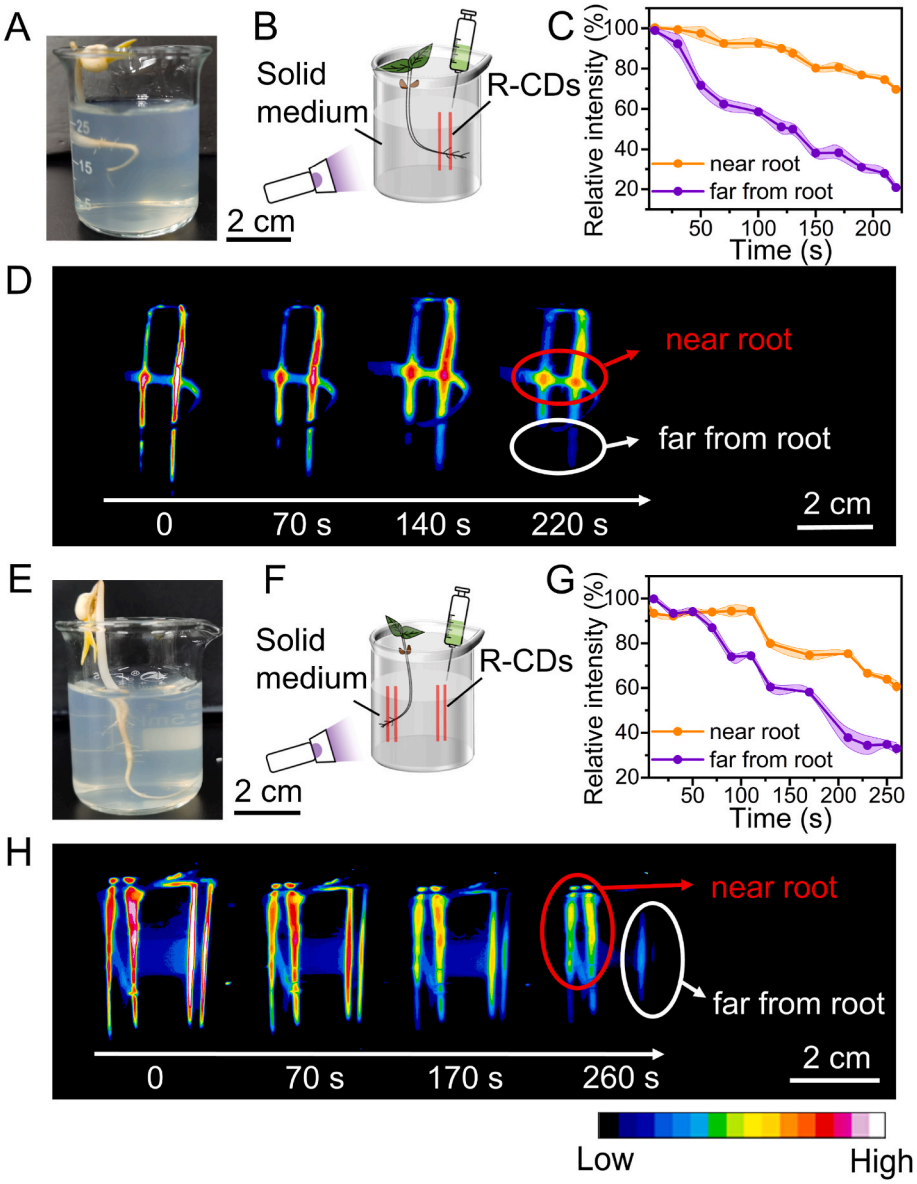

Fig. 6. Images of R-CDs detection of Cu^{2+} on Z-axis (A–D) and X-axis (E–H) directions in medium. (A) and (E) are images of test samples under white light; (B) and (F) are schematic diagrams of the treatments; (C) and (G) are time profiles of fluorescence intensities of R-CDs over the entire process; (D) and (H) are images of R-CDs injected in the medium (The concentration of Cu^{2+} was 30 nM) over time under 420 nm excitation. The red and white circles represent the measurement points for collecting fluorescence intensities at the sites that are near root and far from root, respectively. The shaded regions in (C) and (G) represent the standard deviation from three times sampling.

3. Conclusions

Plant nanobiotechnology is expected to provide solutions to alleviate global agriculture problems. For example, plant nanosensors can communicate the stress on plants in real time under non-destructive conditions, which is conducive to achieving precision agriculture. We have developed biosensors based on R-CDs for the detection of Cu^{2+} in plants. We constructed a user-friendly sensing platform by using carbon dots (CDs) as the optical probe, electronic devices for image acquisition, and a built-in algorithm program for image processing to visually detect Cu^{2+} *in vivo* and *in vitro*. R-CDs can enter plants through co-culture and accumulate in the vicinity of vascular bundles to detect Cu^{2+} in the plant. The sensing platform can image the absorption of Cu^{2+} in plants through fluorescence signal readout. In the application of environmental detection *in vitro*, Cu^{2+} can be visually detected by mapping the fluorescence changes of R-CDs. Through the collaborative detection of Cu^{2+} *in vivo* and *in vitro*, we can more intuitively observe the absorption of Cu^{2+} by plants, which is conducive to understanding plant growth. Moreover, the Cu^{2+} detection function of R-CDs can be applied in a variety of plants/tissues (such as bean sprouts, spinach, and onion tissues), which provides a basis for the application of plants in laboratory research and field cultivation and extends the application of optical nanosensors in real-time plant health monitoring.

CRediT authorship contribution statement

Junjie Lin: Conceptualization, Methodology, Formal analysis, Writing – original draft, Software, Writing – review & editing. **Xiaoman Huang:** Formal analysis, Software, Writing – original draft, Writing – review & editing. **Erfeng Kou:** Conceptualization, Methodology, Writing – review & editing. **Wenxiao Cai:** Formal analysis, Software, Writing – review & editing. **Haoran Zhang:** Investigation, Writing – review & editing. **Xuejie Zhang:** Writing – review & editing. **Yingliang Liu:** Writing – review & editing. **Wei Li:** Conceptualization, Supervision, Writing – original draft, Writing – review & editing, Funding acquisition. **Yinjian Zheng:** Formal analysis, Writing – review & editing. **Bingfu Lei:** Conceptualization, Supervision, Writing – review & editing, Funding acquisition.

Declaration of competing interest

The authors declare that they have no known competing financial

interests or personal relationships that could have appeared to influence the work reported in this paper.

Data availability

Data will be made available on request.

Acknowledgement

The present work was supported by the National Natural Science Foundations of China (Grant No. 12274144; Youth Science Foundation Project, Grant Nos. 52102042), the Project of GDUPS (2018) for Prof. Bingfu LEI, the Guangdong Provincial Special Fund for Modern Agriculture Industry Technology Innovation Teams (No. 2022KJ22, 2023KJ122), Guangdong Basic and Applied Basic Research Foundation (2022A1515010452, 2022A1515010229), and the Guangdong Provincial Science & Technology Project (No. 2020A1414010049), the Elite Youth Program of the Chinese Academy of Agricultural Sciences (Yinjian Zheng).

Appendix A. Supplementary data

Supplementary data to this article can be found online at https://doi.org/10.1016/j.bios.2022.114848.

References

Adamchuk, V.I., Hummel, J.W., Morgan, M.T., Upadhyaya, S.K., 2004. Agr 44, 71–91.
Ahmed, H.B., Abualnaja, K.M., Ghareeb, R.Y., Ibrahim, A.A., Abdelsalam, N.R., Emam, H.E., 2021. J. Colloid Interface Sci. 604, 15–29.
Ahn, T.I., Yang, J., Park, S.H., Im, Y., Lee, J.Y., 2021. J. Clean. Prod. 298, 126747.
Bandi, R., Dadigala, R., Gangapuram, B.R., Guttena, V., 2018. J. Photochem. Photobiol., B 178, 330–338.
Bersier, P.M., Howell, J., Bruntlett, C., 1994. Analyst 119, 219–232.
Bozkurt, E., Bayraktutan, T., Acar, M., Toprak, M., 2013. Spectrochim. Acta, Part A 101, 31–35.
Chen, J., Li, Y., Lv, K., Zhong, W., Wang, H., Wu, Z., Yi, P., Jiang, J., 2016. Sens. Actuators, B 224, 298–306.
Chen, Y., Sun, X., Wang, X., Pan, W., Yu, G., Wang, J., 2020. Spectrochim. Acta, Part A 233, 118230.
Dong, R., Yao, Y., Li, D., Zhang, H., Li, W., Molokee, M., Liu, Y., Lei, B., 2020. Sens. Actuators, B 321, 128643.
Du, J., Yang, Y., Shao, T., Qi, S., Zhang, P., Zhuo, S., Zhu, C., 2021. J. Colloid Interface Sci. 587, 376–384.
Dubey, S., Shri, M., Gupta, A., Rani, V., Chakrabarty, D., 2018. Environ. Chem. Lett. 16, 1169–1192.
Fichman, Y., Miller, G., Mittler, R., 2019. Mol. Plant 12, 1203–1210.
Ge, J., Shen, Y., Wang, W., Li, Y., Yang, Y., 2021. J. Environ. Chem. Eng. 9, 105081.
Gedda, G., Lee, C., Lin, Y., Wu, H., 2016. Sens. Actuators, B 224, 396–403.
Holá, K., Sudolská, M., Kalytchuk, S., Nachtigallová, D., Rogach, A.L., Otyepka, M., Zbořil, R., 2017. ACS Nano 11, 12402–12410.
Hossain, M.A., Piyatida, P., Da Silva, J.A.T., Fujita, M., 2012. J. Bot. 2012, 1–37.
Jin, M.F., You, M.X., Lan, Q.Q., Cai, L.Y., Lin, M.Z., Luo, Z.B., Luo, Z.B., 2021. Plant Biol. 23, 777–784.
Kin, C., Ng Timothy, J., Garner, 2016. Appl. Spectrosc. 47, 241–243.
Kupper, H., Andresen, E., 2016. Metallomics 8, 269–285.
Lew, T.T.S., Koman, V.B., Silmore, K.S., Seo, J.S., Gordiichuk, P., Kwak, S., Park, M., Ang, M.C., Khong, D.T., Lee, M.A., Chan-Park, M.B., Chua, N., Strano, M.S., 2020. Native Plants 6, 404–415.
Li, D., Li, W., Zhang, H., Zhang, X., Zhuang, J., Liu, Y., Hu, C., Lei, B., 2020a. ACS Appl. Mater. Interfaces 12, 21009–21019.
Li, J., Wu, H., Santana, I., Fahlgren, M., Giraldo, J.P., 2018a. ACS Appl. Mater. Interfaces 10, 28279–28289.
Li, N., Diao, W., Han, Y., Pan, W., Zhang, T., Tang, B., 2014. Chem. Eur J. 20, 16488–16491.
Li, W., Wu, S., Zhang, H., Zhang, X., Zhuang, J., Hu, C., Liu, Y., Lei, B., Ma, L., Wang, X., 2018b. Adv. Funct. Mater. 28, 1804004.
Li, X., Zhao, S., Li, B., Yang, K., Lan, M., Zeng, L., 2021. Coord. Chem. Rev. 431, 213686.
Li, Y., Zhang, H., Yao, Y., Gong, T., Dong, R., Li, D., Liu, Y., Lei, B., 2020b. Microchim. Acta 187, 347.
Liang, W., Wang, P., Meziani, M.J., Ge, L., Yang, L., Patel, A.K., Morgan, S.O., Sun, Y., 2021. Nanoscale Adv. 3, 4186–4195.
Liu, C., Tang, B., Zhang, S., Zhou, M., Yang, M., Liu, Y., Zhang, Z., Zhang, B., Pang, D., 2018. J. Phys. Chem. C 122, 3662–3668.
Liu, L., Qin, K., Yin, S., Zheng, X., Li, H., Yan, H., Song, P., Ji, X., Zhang, Q., Wei, Y., Zhao, L., 2021. Photochem. Photobiol. 97, 574–581.
Lu, L., Xie, R., Liu, T., Wang, H., Hou, D., Du, Y., He, Z., Yang, X., Sun, H., Tian, S., 2017a. Chemosphere 175, 356–364.
Lu, S., Sui, L., Liu, J., Zhu, S., Chen, A., Jin, M., Yang, B., 2017b. Adv. Mater. 29, 1603443.
Lu, W., Jiao, Y., Gao, Y., Qiao, J., Mozneb, M., Shuang, S., Dong, C., Li, C., 2018. ACS Appl. Mater. Interfaces 10, 42915–42924.
Moradi, S., Sadrjavadi, K., Farhadian, N., Hosseinzadeh, L., Shahlaei, M., 2018. J. Mol. Liq. 259, 284–290.
Neethu, T.M., Dubey, P.K., Kaswala, A.R., 2018. Int. J. Curr. Microbiol. App. Sci. 7, 3155–3162.
Nie, H., Li, M., Li, Q., Liang, S., Tan, Y., Sheng, L., Shi, W., Zhang, S.X., 2014. Chem. Mater. 26, 3104–3112.
Nissler, R., Mueller, A.T., Dohrman, F., Kurth, L., Li, H., Cosio, E.G., Flavel, B.S., Giraldo, J.P., Mithofer, A., Kruss, S., 2022. Angew. Chem., Int. Ed. 61, e202108373.
Ouzounidou, G., 1994. Environ. Exp. Bot. 34, 165–172.
Pan, L., Sun, S., Zhang, L., Jiang, K., Lin, H., 2016. Nanascale 8, 17350–17356.
Pan, X., Li, D., Fang, Y., Liang, Z., Zhang, H., Zhang, J.Z., Lei, B., Song, S., 2020. J. Phys. Chem. Lett. 11, 1822–1827.
Ragaveena, S., Shirly Edward, A., Surendran, U., 2021. Rev. Environ. Sci. Biotechnol. 20, 887–913.
Rasheed, T., Nabeel, F., Shafi, S., 2019. J. Mol. Liq. 282, 489–498.
Salah, S.A., Barrington, S.F., 2006. Agric. Water Manag. 82, 177–192.
Saleh, S.M., Ali, R., Hegazy, M.F., Alminderej, F.M., Mohamed, T.A., 2020. J. Mol. Liq. 302, 112558.
Steffen, W., Richardson, K., Rockström, J., Cornell, S.E., Fetzer, I., Bennett, E.M., Biggs, R., Carpenter, S.R., de Vries, W., de Wit, C.A., Folke, C., Gerten, D., Heinke, J., Mace, G.M., Persson, L.M., Ramanathan, V., Reyers, B., Sörlin, S., 2015. Science 347, 6223.
Su, Y., Shi, B., Liao, S., Qin, Y., Zhang, L., Huang, M., Zhao, S., 2016. Sens. Actuators, B 225, 334–339.
Tang, H., Zhang, L., Hu, L., Zhang, L., 2014. J. Plant Growth Regul. 33, 195–201.
Thounaojam, T.C., Panda, P., Mazumdar, P., Kumar, D., Sharma, G.D., Sahoo, L., Sanjib, P., 2012. Plant Physiol. Biochem. 53, 33–39.
Wang, W., Wu, K.J., Vellaisamy, K., Leung, C.H., Ma, D.L., 2020. Angew. Chem., Int. Ed. 59, 17897–17902.
Wang, Y., Chang, Q., Hu, S., 2017. Sens. Actuators, B 253, 928–933.
Wei, S., Yin, X., Li, H., Du, X., Zhang, L., Yang, Q., Yang, R., 2020. Chem. Eur J. 26, 8129–8136.
Wong, M.H., Giraldo, J.P., Kwak, S., Koman, V.B., Sinclair, R., Lew, T.T.S., Bisker, G., Liu, P., Strano, M.S., 2017. Nat. Mater. 16, 264–272.
Wu, H., Nißler, R., Morris, V., Herrmann, N., Hu, P., Jeon, S., Kruss, S., Giraldo, J.P., 2020. Nano Lett. 20, 2432–2442.
Xu, Q., Pu, P., Zhao, J.G., Dong, C.B., Gao, C., Chen, Y.S., Chen, J.R., Liu, Y., Zhou, H.J., 2015. J. Mater. Chem. 3, 542–546.
Yan, X., Song, Y., Zhu, C., Li, H., Du, D., Su, X., Lin, Y., 2018. Anal. Chem. 90, 2618–2624.
Zarco-Tejada, P.J., Camino, C., Beck, P.S.A., Calderon, R., Hornero, A., Hernández-Clemente, R., Kattenborn, T., Montes-Borrego, M., Susca, L., Morelli, M., Gonzalez-Dugo, V., North, P.R.J., Landa, B.B., Boscia, D., Saponari, M., Navas-Cortes, J.A., 2018. Native Plants 4, 432–439.
Zhai, W., Wang, C., Yu, P., Wang, Y., Mao, L., 2014. Anal. Chem. 86, 12206–12213.
Zhang, X., Shiraishi, Y., Hirai, T., 2007. Org. Lett. 9, 5039–5042.